TECHNICAL UNIVERSITY OF CLUJ-NAPOCA

ACTA TECHNICA NAPOCENSIS

Series: Applied Mathematics, Mechanics, and Engineering
Vol. 69, Issue I, March, 2026

CONSIDERATIONS ON ORDER ANALYSIS AND FAULT DETECTION ON A SPEED REDUCER WITH HELICAL GEARS

Iulian LUPEA

Abstract: *Fault diagnosis on a test rig with a speed reducer and helical gears is observed by using order analysis. The vibration is monitored on the reducer housing with a triaxial accelerometer. Various speed profiles are imposed with the variable frequency drive and tracked with a tachometer. Three load levels are imposed with a magnetic powder brake. Based on colormaps, orders and power spectrum peaks were assigned to the associated machine elements of the speed reducer, the AC motor, and shafts. GMFs for the first and the second gear pairs, their harmonics, the frequency peaks of the input and output reducer's shafts, the kurtosis value and sideband energy ratio were considered to detect a fault in the helical pinion of the first stage of the reducer and the misalignment at the interface between the speed reducer and the powder brake.*

Keywords: *Order analysis, vibration-based condition monitoring, speed reducer, helical gear fault.*

1. INTRODUCTION

One of the most valued methods for evaluating the operational state of machine components and machine condition monitoring (MCM) in power generation, transportation systems, and industrial manufacturing is vibration analysis. The type of defect, how it develops, and the machine elements' functioning parameters all affect the vibration signature that is gathered from the measurement sites. For noise, vibration, and harshness (NVH) testing as well as for evaluating noise and vibration signals of rotating or reciprocating machinery in the frame of the MCM for which the rotational speed varies over time, order analysis (OA) is a vital technique [1], [2], [3], and [4].

Finding the sources of undesired noise and vibrations, distinguishing speed-related vibrations from structural vibrations and resonances, identifying essential machine speeds, and identifying defective parts are all made easier with the use of OA in MCM applications and NVH investigations. OA can be used in wind turbine planetary gearboxes, automobile and aircraft engines, automobile transmission units, compressors, pumps, speed reducers, and other devices where the frequency produced by different machine components varies according to the rotating speed of a reference machine element.

A tachometer, a toothed or notched encoder, or an in situ MEMS accelerometer that decomposes the time-varying gravity acceleration are typically required to detect the instantaneous speed of a machine's reference spinning shaft [5]. With some rotational speed parameters known in advance, tachless rotational speed can be approximated; alternatively, the detection of rotational speed can be totally automated, beginning with the vibration signal produced by a gear pair [6]. The instantaneous speed is then linked with the vibration and noise signals. An order is a harmonic of the machine element's rotating speed in a system. As a result, we concentrate on revolutions rather than time and on orders

Received: 30.01.26; **Similarities**: 17.02.26: **Reviewed**:23.02./25.02.26: **Accepted** 17.03.26.

rather than frequency in the spectrum domain. Order-related information, such as the order power spectrum, can be computed continuously or offline using OA. Other popular applications include spectral map analysis, order tracking, angular resampling, order waveform extraction, and tachometer processing [7], [8].

As the machine runs, each component produces a distinct vibration and noise profile, which adds in a particular way to the machine's overall vibration and noise. Gear, bearing, belt, shaft, or other machine element faults change the mechanical transmission's typical operating conditions, increasing vibration and lowering transmission quality or machine failure [9]. Normal or malicious machine activity, as well as manufacturing or mounting flaws, can result in faults.

The FFT power spectrum may correctly connect certain frequency components with particular mechanical elements when the rotation speed is consistent and the time waveform samples are equally spaced in time. When the rotational elements' speed varies, the FFT power spectrum for even time-spaced samples gets hazy, blurring the distinct frequencies in the frequency domain. Angle intervals between adjacent samples increase with shaft rotation speed during a run-up test and vice versa during coast-down events. As a result, it is impossible to pinpoint any frequency components (peaks) connected to specific mechanical components. Machine element problems are frequently indicated by frequency lines of the spectrum; however, after frequency smearing, frequency lines are no longer reliable indications of defects.

Vibration signals from rotating and reciprocating devices with changing speeds are analyzed using the order spectrum instead of the frequency spectrum. By employing the order tracking technique, the equal angle interval resampling (angular resampling) of the obtained vibration signal can transform the nonstationary signal in the time domain into a stationary signal in the angle domain [10], [11].

For minor nonstationary vibration signals or slight speed variations, the short-time Fourier transform (STFT) may be appropriate. The windowed signal block should remain relatively stationary throughout the window interval if the window length is sufficiently short. The windowed signal block should have a sufficient number of samples to allow for a suitable frequency resolution from the applied Fourier transform. The analysis's temporal resolution decreases with the size of the signal block. Because the STFT makes use of the fast Fourier transform (FFT), it is computationally efficient. Joint time-frequency analysis (JTFA) overcomes the FFT power spectrum limitation for nonstationary signals by providing information in both the time and frequency domains [12].

OA is advised when measuring the rotational speed of reciprocating and rotating equipment. In order to achieve the same signal resampled according to the rotating speed (the so-called synchronous sampling rate), we must modify the sampling rate (usually software resample) because OA demands even angle samples. Order analysis is then performed on the even-angle signal using the conventional FFT method. More distinct peaks connected to the various mechanical components and the machine as a whole can be seen in the resulting order power spectrum. The tachometer is often used to measure the rotational speed of the shaft vibration, which is typically the first order. In addition to resampling, this article uses the Gabor transform (GT), a sort of invertible time-frequency transform, for OA.

The spectral content of time-varying signals, where the time series vibrations are converted into time-frequency pictures, can be observed using a wide range of mathematical techniques. Excepting the STFT, which is the most basic method, we mention a more precise methods, the GT method (STFT with the window of the Gaussian function profile), that helps you identify the order components in the time-frequency domain when the speed is variable. The inverse Gabor transform is known as Gabor expansion, and GT is a kind of invertible joint time-frequency transform. The Wavelet transform (WT), Stockwell or S-transform, and Wigner-Ville distribution (WVD) [13] are further combined time-frequency transforms that vary in the amount of time and frequency precision that can be achieved.

It is possible to think of orders with amplitude and phase as harmonics of the tracked rotational

frequency. The order tracking approach measures the amplitude and phase of the produced spectrum and tracks the frequency changes of the orders of interest over time. When diagnosing faults in rotating machinery, this method is frequently employed [14], [15], and [16]. In order to identify and classify errors, order tracking for time-varying speed machines can be utilized for parameter extraction and applied to deep learning neural network architectures, artificial neural networks, and classical machine learning approaches [17], [18].

While certain gear flaws, such as cracks, spalling, and pitting, are localized, others involve all active tooth flanks and result in gear wear [9], [19]. Due to meshing forces or repeated shocks when the mating teeth engage and come into contact, certain vibrations are also produced during regular gear operation.

In particular, certain frequency components, such as the gear mesh frequency (GMF), their harmonics, and related sidebands, can be used to infer gear failures in frame of order analysis, particularly order tracking. The effects of amplitude and frequency modulation are combined to create symmetrical families of sidebands that are equally spaced around a center frequency due to a defect on the gear's flank. The two amplitudes of a sideband pair may be asymmetric with respect to the fundamental frequency or their harmonics due to the combination of the sidebands (AM and FM); sideband amplitudes may be larger than the fundamental frequency, or it may even be the case with an undetectable fundamental frequency from the spectrum [1], [20], and [21]. A logarithmic spectrum scale is necessary due to the low amplitude levels of GMFs, their harmonics, and sidebands for nascent localized faults.

Additionally, vibrations are produced by AC induction motors. Separating the origins of vibration, which might come from mechanical or electrical causes such misalignment or imbalance, is one part.

In this article we focused on OA for gear fault detection on a speed reducer with helical gears. The OA is performed on a test rig that includes the AC motor with variable frequency drive, the speed reducer and a magnetic powder brake. Run-up, coast-down tests, and constant speed waveforms were recorded for several different loads and off-line analyzed. Vibration patterns and orders of the speed reducer components are identified. A fault on a helical gear and shafts misalignment have been detected. Comments on the condition monitoring of the device are formulated.

2. THE TEST RIG WITH SPEED REDUCER AND ACQUISITION SYSTEM

The experimental test rig is based on a speed reducer gearbox actuated by a three-phase AC motor which creates a smoother and powerful rotation with few vibration-related issues. A variable frequency drive (VFD) as the motor speed regulator and a magnetic powder brake

Fig. 1. The test rig: AC motor, VFD, speed reducer, magnetic powder brake

are components of the test rig (Figure 1), along with the acquisition system. The VFD permits reversal by electronically changing the phase sequence of voltage applied to the motor and controls the speed by varying the frequency of the motor input signal. The motor type is MS 90S-4, 1.1kW, three phase asynchronous induction motor with aluminum housing, with 1400 rpm nominal rotational speed and 4 poles. The test rig base stiffness was not tested for the fulfillment of the "Massive Foundation" criteria defined by API 541 (stating that the vibration near the motor feet be less than 30% of the vibration measured at the motor bearing) [22],[23]. Here, the motor is suspended and connected via a flange to the speed reducer. The motor generates small vibrations due to minor rotor imbalances and misalignment; there are no bearing defects. Slight vibrations are generated from structural (natural) resonances of the motor housing or the shaft with the rotor

that are within acceptable industry limits. For this motor, ISO 10816-3 standard, limits the vibration velocity to 4.5 mm/s RMS, under flexible foundations. On the other hand, motor vibrations can be caused by electrical faults such as unbalanced supply voltage, winding faults, and uneven air gaps or electromagnetic forces. A common frequency peak in the electrical motor spectrum is the slip frequency. This comes from the difference between the speed of the rotating magnetic field and the actual rotor's rotating speed (which is less than the speed of the rotating magnetic field due to the load and inertia). Some other common frequencies are the electrical line frequency, the rotor bar pass frequency and the pole pass frequency. Delta VFD drive maintains stable, vibration-free motor operation.

Fig. 2. Sensors: a) tachometer pointing area; b) triaxial accelerometer

A NI USB-4431 acquisition, 24 bits, 102.4 kS/s dynamic acquisition board is used, with all four analog channels. The tachometer's laser beam is aimed at the AC motor fan, where one piece of reflecting tape is attached (Fig. 2a). A triaxial IEPE piezoelectric accelerometer (101mV/g) is glued laterally (Fig. 2b) on the reducer gearbox case at the level of the input shaft bearings. The X-axis is along the input shaft facing the magnetic brake, the Y-axis radially downwards and the Z-axis also radially. The load on the output shaft is carried out by the electromagnetic powder brake with three main components: the rotor connected to the output reducer shaft, the coil and the stator. The magnetic field inside the coil changes in proportion to the electrical curent and alter the viscosity of the special powder placed between the stator and the rotor. The powder particles align along magnetic field lines. A curent regulator for powder brake (based on a Taurus-BX card) and the associated control circuit is shown in Figure 3. The voltage is imposed through a potentiometer and the current intensity through the brake is observed.

The braking torque is proportional to the magnetic field strength, which depends on the applied DC input current.

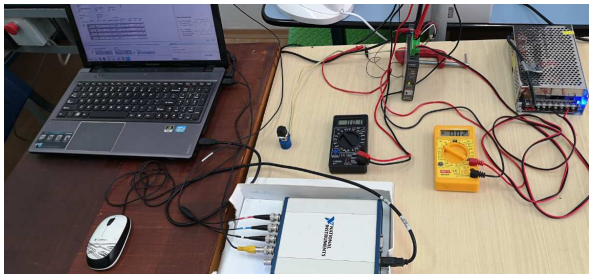

Fig. 3. The acquisition system and the magnetic powder brake curent regulator

3. ODER ANALYSIS FOR THE GEARBOX REDUCER

The speed reducer with two gear pairs (p1 and p2) is schematized in Figure 4. The relation between the input and output turning speed is as follows (1):

$$i_{in} \cdot \frac{19}{51} \cdot \frac{17}{66} = i_{out} \qquad \text{or:} \qquad (1)$$

$$i_{in} = i_{out} \cdot \frac{51}{19} \cdot \frac{66}{17} \qquad (2)$$

resulting the speed reducer ratio r=10.421

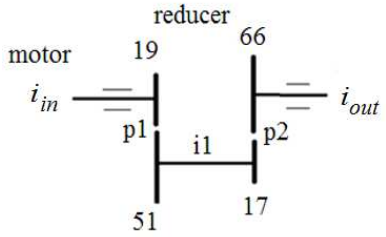

Fig. 4. Speed reducer kinematic chain

A LabVIEW data logging application is run with acquisition on four analog channels, three of them for the triaxial accelerometer mounted laterally on the gearbox housing and the fourth analog channel for acquisition of tachometer voltage pulses (one pulse per shaft revolution). The sampling rate is 10 kHz resulting the frequency bandwidth of 5 kHz. The sampling

rate and the calculated orders are related according to the equation (3):

$$f_s = 2.56 \cdot o_{\max} \cdot i_{in\_\max} \quad (3)$$

where $o_{\max}$ is the maximum order of interest and $i_{in\_\max}$ is the maximum rotational speed of the reducer input shaft [7].

In the LabVIEW acquisition application, sampling per input channel being 5000 (samples) results in two readings per second with the DAQmx Read.vi function. The data is saved in a log file. DAQmx Read.vi returns a 1D array of four waveforms (dt = 0.0001 seconds), each waveform corresponding to an input channel. A typical acquired waveform from the accelerometer is depicted in Figure 5. The speed (RPM - revolutions per minute)

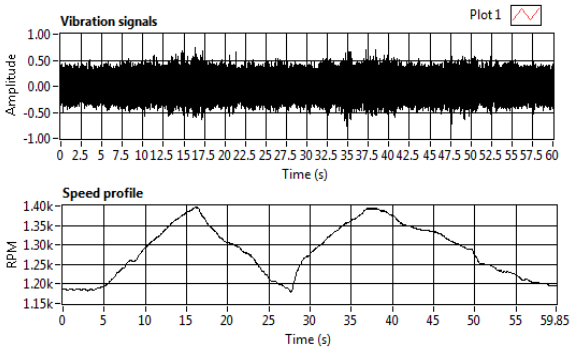

Fig. 5. Acquired vibration waveform (Y axis) and the input shaft speed profile

profile as a function of time can be seen, observing two consecutive run-up and coast-down portions. The recording time is 60

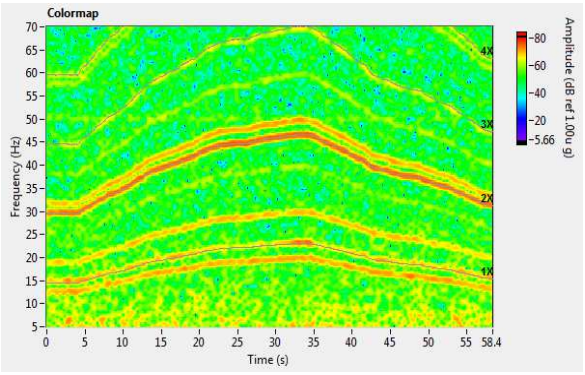

Fig. 6. First four input shaft orders (1X,...,4X) - variable speed

seconds of continuous acquisition and simultaneous sampling on the four channels. A second application is loading the logged data and by resampling method, OA is performed offline. The three-dimensional colormap diagram (intensity graph) as the first step in OA with frequency versus time (60 seconds) is shown in Figure 6. The maximum vibration level (acceleration [g]) is 80 dB for a reference value of 1*10^-6 [g]. The applied RMS averaging generated good results of the overall spectrum, the acquired signals being with

Fig. 7. P1 pinion on reducer input shaft and support bearings

various order components.

The colormap shows the amplitude of the vibration spectrum in increasing steps from blue to red, depending on frequency or order. The amplitude of the vibration can be observed as a function of rotation speed or time. Initially the conversion of the recorded signal with fixed time sampling rate into an even angle signal with a constant number of samples per input shaft revolution took place; therefore, at higher revolution speeds, the signal is sampled faster (the signal was converted from time domain to angle domain). The Fourier transformation of the resampled signal results directly in an order spectrum. The analysis window contains the same number of signal samples at each sampling point. FFT is applied to angle blocks that has an angle duration. The analysis can be limited to the order range of interest for reducing the processing time. OA avoids spectral smearing when observing non-stationary vibration signals since rotational harmonic components stay at fixed order positions in order spectra. Angle blocks are averaged. FFT spectra are appropriate to be phase-aligned before averaging (all spectra are

related to the same initial angular position). This leads to the reduction of unwanted random noise content [11]

3.1. Reduce input shaft orders:

The first order (1X) is associated to the revolution speed of the reducer input shaft, on which P1 pinion (Fig.7) is mounted, and is well observed in the intensity graph shown in Figure 6. This order helps find a possible fault in the P1 pinion by modulating the gear mesh

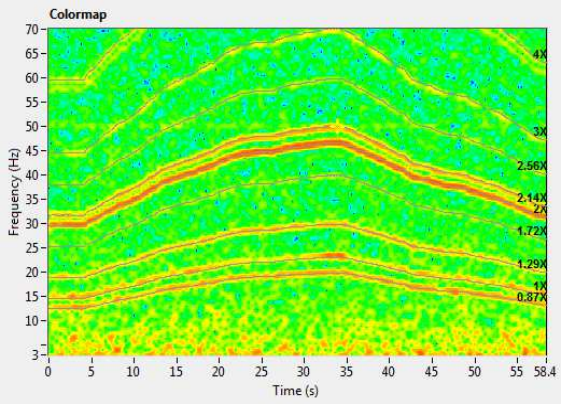

Fig. 8. Evenly spaced orders - 0.42X apart

frequency. The magnitude of the signal energy at time t and frequency f is expressed by the

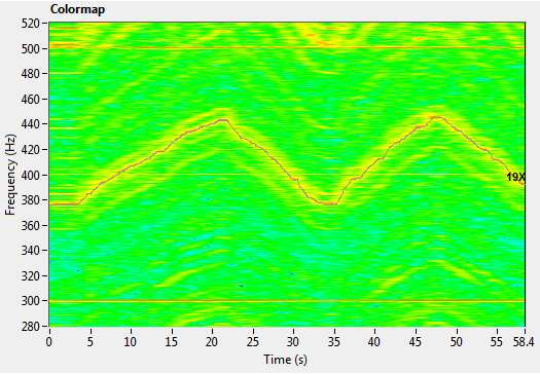

Fig. 9. Order 19X (first gear pair GMF) and two harmonics of the power line

color. From red to blue the energy varies from strongest to weakest. As well, one can see how the spectral content evolves over time and with the speed variation. The second harmonics (2X) is highly pronounced. The third (3X) and fourth (4X) harmonics are less pronounced.

In Figure 8, orders 0.87X, 1.29X, 1.72X, 2.14X and 2.56X are evenly spaced with an interval of about 0.42X. These are subharmonics of the main shaft.

3.2. Gear mesh frequencies and sidebands

The 19th order (19X), shown in Figure 9, corresponds to the GMF of the first gear pair Z19/ Z51, a variable speed recording and load level L0:

$$GMF_{19/51} = Iin \cdot 19 \qquad (4)$$

Associated sidebands for a constant speed record are shown in Figure 10. GMF of the second stage, gear pair Z17/ Z66, is poorly visible along order 6.33 X (Figure 13):

$$GMF_{17/66} = i1 \cdot 17 = Iin \cdot 19/51 \cdot 17 \qquad (5)$$

There are no faults in the gear pair of the reducer second stage.

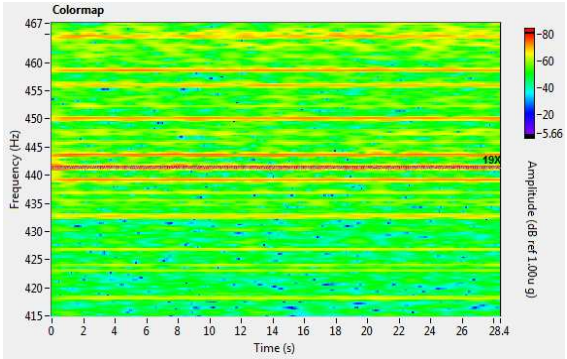

Fig. 10. Test rig: 19 X order (GMF of first gear pair with sidebands - constant speed

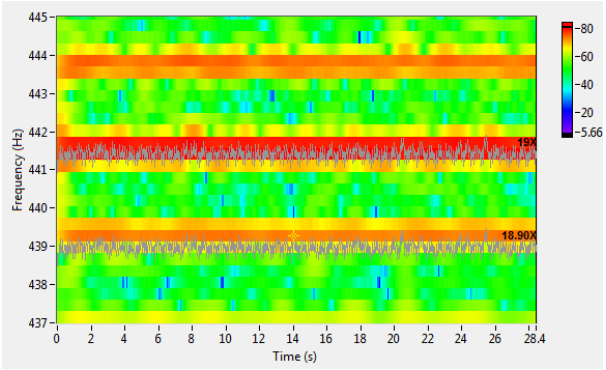

Fig. 11. Nearest pair of side bands of 19X order - output shaft missalignment fault

At 300 Hz and 500 Hz, horizontal lines can be observed on the spectrum versus time in Figure 9. These frequency values are not sensitive to the rotational speed and represent harmonics of the frequency line (electrical power). The set of such frequency lines comprises more visible horizontal lines at 100Hz, 300Hz, 400Hz, 500Hz and 600Hz.

Structural resonances are at constant frequency but have a different appearance than these.

In Figure 11, for a record with constant speed, the nearest sideband pair about the GMF1 (19X order) is given by the modulation of the signal coming from the out shaft of the reducer. The tachometer indicates a constant speed of 1394 rpm or 23.23 rps [Hz]. The reducer output shaft rotational speed is 2.229 Hz (6):

$$i_{out} = i_{in} \cdot \frac{1}{r} \tag{6}$$

The nearest pair of side bands must have the lower (i_{sbL}) and upper (i_{sbU}) band at 439.141 (18.9X) and 443.599 (19.1X) respectively (7), proving the modulation of the GMF frequency with the reducer output shaft rotational speed.

$$\begin{aligned} i_{sbL} &= i_{in} \cdot Z_1 - i_{out} \\ i_{sbU} &= i_{in} \cdot Z_1 + i_{out} \end{aligned} \tag{7}$$

The intensity graph shown in Figure 11 proves the relatively large misalignment between the reducer output shaft and the shaft connected to the rotor of the magnetic powder brake.

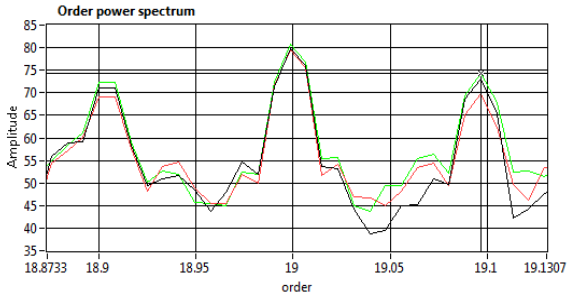

Fig. 12. Order Power spectrum - nearest pair of side bands of 19X, RMS ave, speed=ct

The order power spectrum of a waveform recorded at the highest available constant speed, 30-second duration, and L3 load is shown in Figure 12. Here we have the power spectrum with the closest pair of sidebands

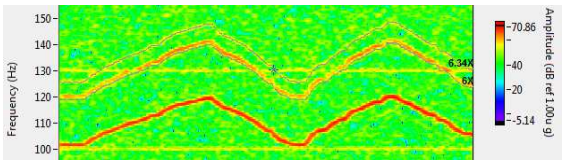

Fig. 13. Order 6.33X associated to $GMF_{17/66}$ and AC motor fan 6X order.

around the 19X order, with RMS average, block size of 20480 and linear weighting mode. Linear averaging is suitable for constant rotational speed or small subsets of the dataset for which the average level can be assumed almost constant while exponential averaging is appropriate for non-stationary signals that place more emphasis on newer samples.

The orders of the AC motor are present in the colormap but are of little interest in the current study. The AC motor fan has six pales. The associated 6X order is visible (Figure 13) and the next two harmonics are faintly visible.

3.3. Fault on helical pinion P1 and GMF sidebands

A fault on an active flank of the pinion P1 was artificially created (Figure 14).

The first signs of localized faults on gear

Fig. 14. Fault on the pinion flank

flank are given by indicators that measure signal impulsiveness or "peakedness" such as kurtosis and crest factor. Kurtosis (the fourth centralized moment of the signal, normalized by the square of the variance) on X and Y

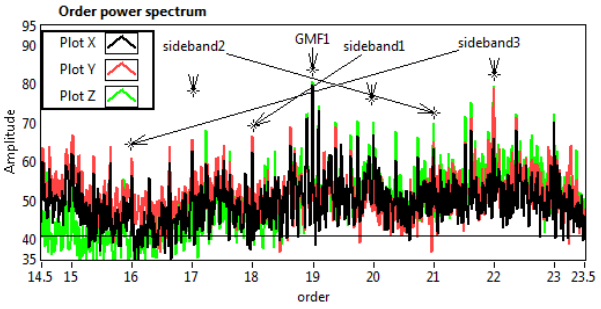

Fig. 15. GMF of p1 gear pair and 3 sidebands pairs associated to faulty helical pinion P1

accelerometer axes is between 3 and 4 (3 is the reference value for a random signal with Gaussian distribution) and exceeds the value 6

on the Z axis for all measurements, regardless of the speed variation. This indicates a source of impulsiveness that could be wear or damage to gear teeth. We observe the effect of the created fault on the power spectrum. Defects, their shapes, or the manufacturing errors of

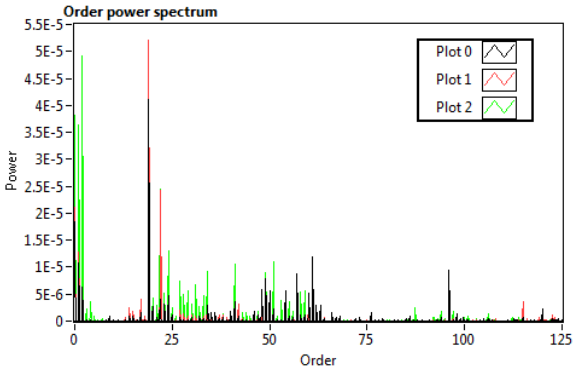

Fig. 16. Order power spectrum - first 125 orders, vector averaging, order rezolution=0.1, linear scale

gears are encoded into the GMFs, harmonics, and their sidebands in the frequency domain. The number and the amplitude of the sidebands are often correlated with the severity of the gear fault. The greater the fault severity, the higher the ratio of sidebands energy to central

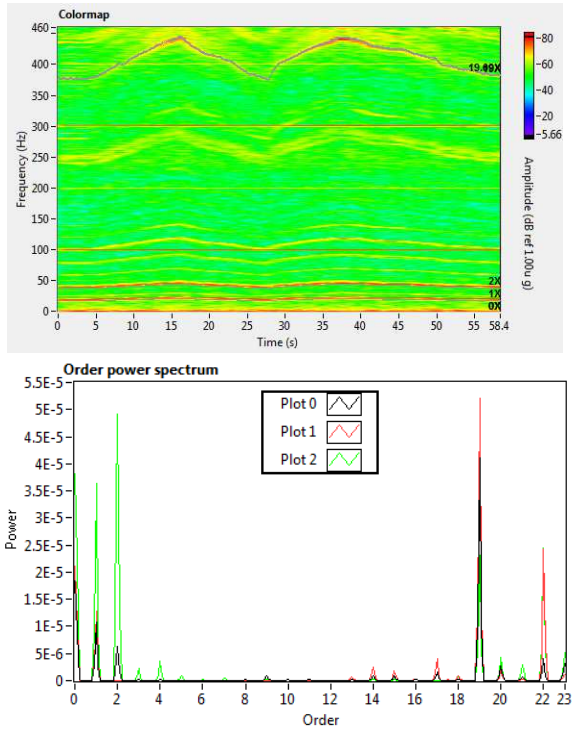

Fig. 17. Order power spectrum peaks and the colormap for 1X, 2X and 19X orders

frequency energy. The appearance of the second pair of lateral bands can also be observed. For localized defects on the gear from the modulation process, the resulting sidebands (at the faulty gear rotational frequency) are hardly discernible in the spectrum [20]. Three sidebands of the GMF of the gear pair p1, for all three accelerometer axes and for the total duration (60s) of the waveform recording are shown in Figure 15. The largest peak of a sideband pair is the right side of sideband3 on Y axes (red color). Sidebands originate from the amplitude modulation of the gear mesh signal as the damaged tooth comes in and out of contact with the driven gear once per revolution of the input shaft. The order power spectrum (dB) (Figure 15) is obtained for the entire duration (60s) of the acquired signal (converted to an even-angle signal), Hanning window, Exponential and RMS averaging, number of average blocks of 10 and a large block size of the even-angle signal for good resolution.

3.4. Orders with maximum amplitude and power in band

Based on FFT, the order power spectrum is derived which shows the power spectrum for all orders in the specified time interval. Dominant order magnitude and phase can be observed and dominant and individual order waveforms can be extracted. Gabor transform and expansion (8) is used for time waveform extraction for the selected orders:

$$x(t) = \sum_{m=-\infty}^{\infty} \sum_{n=-\infty}^{\infty} C_{m,n} h_{m,n}(t)$$
$$h_{m,n}(t) = h(t - mT) e^{jn\Omega t} \quad (8)$$

where x(t) is the acquired time signal, $C_{m,n}$ are the Gabor coefficients, $h_{m,n}$ are synthesis functions, T and Ω are time and frequency sampling intervals, respectively. The discrete version of the transformation is used with LabVIEW functions [24], [25].

The first 125 orders of the input shaft have been considered for monitoring the power in orders up to the 6th harmonic of the GMF1. In Figure 16 the order power spectrum with linear scale is shown. The associated frequency interval is up to 2.9 kHz for the 23.23 Hz the

rotational speed of the P1 helical pinion. Vector averaging has been applied and the order resolution is 0.1.

The order power spectrum with orders up to the 23X order is zoomed in Figure 17. The first three largest peaks are at orders 1X, 2X and 19X. An increased magnitude of the first order often indicates imbalance. Phase along with magnitude of the first order can help reduce the imbalance. Power in bands (for a range width of 0.8 orders) for orders 1X, 2X and 19X with sidebands, individually for each sensor axis, are presented in Table 1. The observed record is for variable speed (Figure 17) and L3 load. For Z axis (Table 1) order 19X (GMF1) is not significantly large, being important on the X and Y axes.

Table 1

Power in bands for 19X and sidebands

order no.	order range	X	Y	Z
		powers in bands		
		dB rms, ref 1.0E-6 g		
22X	21.6–22.4	66.24	73.81	73.89
21X	20.6–21.4	58.57	54.29	64.74
20X	19.6–20.4	64.60	63.11	66.45
19X	18.6–19.4	76.13	77.14	73.62
18X	17.6–18.4	53.35	60.02	57.80
17X	16.6–17.4	62.23	66.29	50.28
16X	15.6–16.4	54.18	56.22	51.48
2X	1.6–2.4	68.04	49.59	76.92
1X	0.6–1.4	70.34	71.08	75.61

Powers in bands from Table 1 were calculated with vector averaging, which removes noise and order components (from the signal) that are not synchronous with the running speed. The window type applied to the sample block is Hanning and the order resolution is 0.1 order. Power in bands are listed for comparison and are expressed in dB rms with a reference value of 1.0E-6 [g].

A useful gear mesh condition indicator, that can be monitored over time, is the sideband energy ratio (SER) [26],[27]. This can provide warnings when compared to alarm levels for specific gears. The ratio of the power in 19X order to the sum of the powers in the first three sidebands, from Table 1, is: 80.6dB/78.7dB.

From another point of view by extracting the most significant orders for the largest frequency band of the analysis (up to 5kHz) the most significant orders are in the area of orders 133X, 166X, 173X included in the frequency band 2.5kHz - 4.kHz (Figure 18). We consider that these orders are not in the area of interest and unrelated to the gear faults.

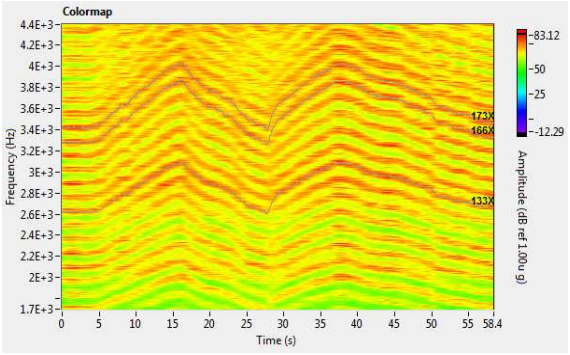

Fig. 18. Area with the most significant orders (133X, 166X, 173X) on Z axis of the record

3.5. Helical gear fault related order waveforms extraction

When OA is performed with Gabor transform, the transformation is invertible. Gabor coefficient are generated by the direct transformation and inverse transformation (Gabor expansion) helps generate the initial time waveform. The 19X order for the faulty P1 helical pinion is selected and by Gabor expansion the identified order is transformed to a time waveform as shown in Figure 19, where

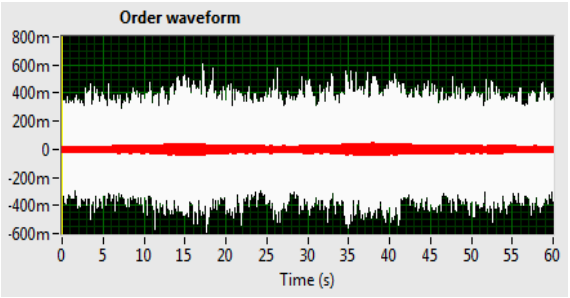

Fig. 19. Waveform for 19X order and entire vibration signal on Y axis

the entire signal is also presented. This order waveform extraction is performed with a bandwidth of 0.8 order and for Y axis of accelerometer. Sets of orders can be selected and the associated order waveforms (in time

domain) are generated using inverse Gabor Transform. The orders associated to the sideband pairs of the 19X order are extracted (as waveforms) and shown in Figure 20. A magnitude correlation can be observed between the extracted waveforms and the peaks in the associated order power spectra (Fig.15) for the same acquired waveform.

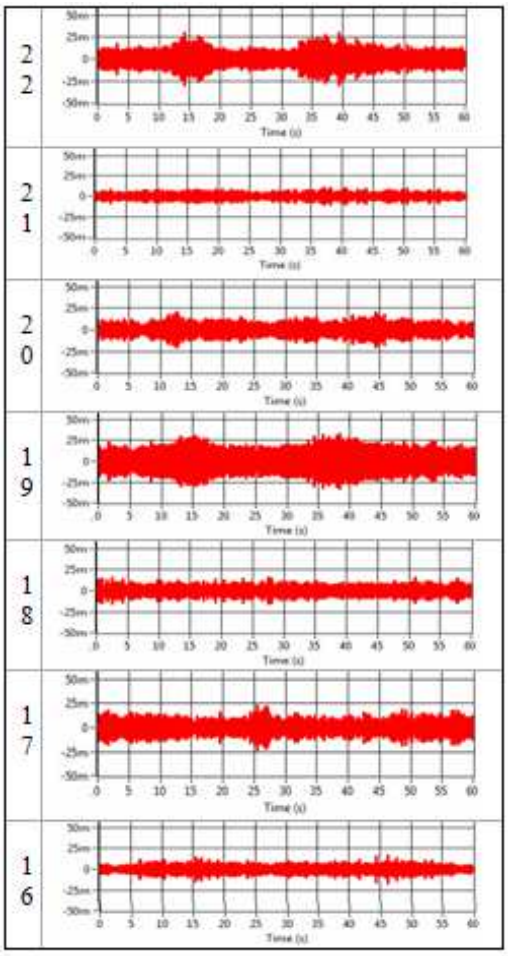

Fig. 20. Extracted waveforms for order 19X and three sideband pairs, bandwidth 0.8 orders, axis Y

4. CONCLUSIONS

Fault diagnosis on a test rig with speed reducer and helical gears is observed by using order analysis. The speed of the three-phase AC motor driving the reducer and the load at the reducer output are controlled. A triaxial accelerometer and a tachometer are used to monitor gearbox vibrations and the rotational speed of the reducer input shaft. Waveforms for several speed profiles (one or two successive run-up and coast-down test profile and also constant speed tests) and three load levels were recorded. Based on the colormaps, order power spectrum peaks for a multitude of orders, the vibrational behavior of some machine elements have been identified. GMF of the first and the second gear pair, their harmonics, the input and output reducer's shafts vibrational patterns, as well as the vibrations of some components of AC motors are identified and discussed. The 19X order associated with the gear mesh frequency, three sidebands pairs and the sideband energy ratio are used to detect the fault in the helical pinion of the first stage of the reducer. Power in bands (separately for each accelerometer axis) of the mentioned orders, and the associated order waveforms extracted with Gabor expansion, help the fault assessment. The presence of these sidebands and the power in bands distribution are indicating the localized fault in one active tooth flank of the mentioned pinion. Order power spectrum was used to evaluate the power on orders and to detect the contribution of the orders to the overall vibration level. The misalignment of the reducer output shaft with the magnetic powder brake is detected by the prominence of the nearest pair of side bands about 19X order, namely 18.9X and 19.1X.

Further studies will pay more attention to the sideband energy ratio of the reducer gear pairs for various speed profiles and load levels. Colormaps and spectrograms will be used to extract features such as the mean instantaneous frequency (MIF), mean instantaneous bandwidth and the group delay. The importance of these features, along with other specific statistical features, will be assessed for machine learning-based fault diagnosis.

5. REFERENCES

[1] Randall, R.B., Vibration-Based Condition Monitoring: Industrial, Automotive and Aerospace Applications, John Wiley & Sons: Hoboken, NJ, USA, 2021.

[2] Scheffer C., Girdhar P., Practical Machinery Vibration Analysis and Predictive Maintenance, First Edition, Newnes, 2004.

[3] Maurice L. Adams, Jr., Rotating Machinery Vibration, CRC Press, 2000.

[4] Mogal, S.P., Lalwani, D.I., *Experimental investigation of unbalance and misalignment in rotor bearing system using order analysis*, Journal of Measurements in Engineering, Vol. 3, Issue 4, 2015.

[5] Li, Y.; Chen, Z.;Wang, L. *A New Order Tracking Method for Fault Diagnosis of Gearbox under Non-Stationary Working Conditions Based on In Situ Gravity Acceleration Decomposition*. Appl. Sci. 14., 2024.

[6] Barrios, M. L. R., Montero, F. E. H., Mancilla, J. C. G., & Marín, E. P. *Tacho-less automatic rotational speed estimation (TARSE) for a mechanical system with gear pair under non-stationary conditions*. *Measurement*, *145*, 480-494, 2019.

[7] Getting Started with Order Analysis, *Toolkit User Manual*, www.ni.com., 2007

[8] Lupea, I., *Considerations on order analysis of a rotating machinery test rig*, Acta Technica Napocensis, Series: Applied Mathematics, Mechanics, and Engineering, Vol. 64, Issue III, 2021.

[9] ISO 10825; *Gears—Wear and Damage to Gear Teeth.,* International Organization for Standardization: Geneve, Switzerland, 2022.

[10] Fyfe,K.,R., Munck,E., *Analysis of computed order tracking*, Mechanical Systems and Signal Processing, 11(2), 1997.

[11] Order Analysis - *Solution User Manual - Order Tracking Analysis* V23-1, www.dewesoft.com 2023.

[12] Bagri, I., Tahiry, K., Hraiba, A., Touil, A., Mousrij, A. *Vibration Signal Analysis for Intelligent Rotating Machinery Diagnosis and Prognosis: A Comprehensive Systematic Literature Review*. Vibration,7, 2024.

[13] Lupea, L., Lupea, M., *Detecting Helical Gearbox Defects from Raw Vibration Signal Using Convolutional Neural Networks*, Sensors, 23, 8769, 2023.

[14] Wang, KS, Feng,K., Zuo,M., *An order spectrum based method to ensure consistent monitoring through Vold-Kalman filter order tracking*, 19th World Conf. Non-Destructive Testing, 2016.

[15] Gade,S., Herlufsen, H., Konstantin-Hansen, H., Vold, H., *B&K, Tech. review: Characteristics of the Vold-Kalman Order Tracking Filter*, www.bksv.com, 1999.

[16] Wu,J-D, Wang, Y., Chiang,P., Bai,M., *A study of fault diagnosis in a scooter using adaptive order tracking technique and neural network*, Expert Systems with Applications, 36, 2009.

[17] Rodrigues, C.E., e.a., *Machine Learning Techniques for Fault Diagnosis of rotating machines using spectrum images of vibration orbits*, www.sba.org.br, 2020.

[18] Zhao, D., Li, J., Cheng,W, *Feature Extraction of Faulty Rolling Element Bearing under Variable Rotational Speed and Gear Interferences Conditions*, Hindawi Publishing Corporation Shock and Vibration, Vol. 2015.

[19] Lupea, I., Lupea, M., *Continuous Wavelet Transform and CNN for Fault Detection in a Helical Gearbox*. Appl. Sci., 15, 950, 2025.

[20] Lupea, I., Lupea, M., Coroian, A., *Helical Gearbox Defect Detection with Machine Learning Using Regular Mesh Components and Sidebands*. Sensors, 24, 3337, 2024.

[21] Lupea, I., Lupea, M., *Fault detection on a rotating test rig based on vibration analysis and machine learning*. *PROCEEDINGS OF THE ROMANIAN ACADEMY*, 2022.

[22] Mistry,R., Finley,W.R., Kreitzer,S., *Induction motor vibrations in view of the API 541- 4th edition*. Material IEEE Paper No. PCIC, 2007.

[23] Finley, W.R., Hodowanec,M., Holter, W., An Analytical Approach to Solving Motor Vibration Problems, IEEE Transactions On Industry Applications, Vol. 36, No. 5, 2000.

[24] Wexler, J., Raz, S., *Discrete Gabor expansions*, *Signal Processing,* vol. 21, no.*3,* pp. 207-221, Nov. 1990.

[25] Shie,Q., Dapang, C., *Discrete Gabor Transform*, IEEE Transactions On Signal Processing, Vol. 41, No. **7,** July 1993.

[26] Dempsey, P.J. *Investigation of Sideband Index Response to Prototype Gear Tooth Damage,* Glenn Research Center, Cleveland, Ohio, *2013, https://ntrs.nasa.gov/ citations/ 20140011094*

[27] M. Zhang, H. Cui, Q. Li et al. *An improved sideband energy ratio for fault diagnosis of planetary gearboxes*, Journal of Sound and Vibration, 491, 2021

Consideraţii cu privire la detectarea defectelor unui reductor cu roţi cilindrice şi dinţi înclinaţi pe baza analizei ordinelor

Rezumat*:* Articolul urmăreşte detectarea defectelor unui reductor cu angrenaje cilindrice, cu dinţi înclinaţi, folosind analiza ordinelor de vibraţii produse de componentele mecanice. Standul de studiu conţine reductorul cu două trepte, comanda in viteză a motorului trifazat şi o frână cu pulbere magnetică comandată. Senzorii folosiţi sunt un accelerometru triaxial şi un tahometru. Sistemul de achiziţie cu patru canale şi eşantionare simultană înregistrează un set de forme de undă la viteză variabilă şi constantă, şi cateva niveluri de sarcină. Este identificat defectul de uzură practicat pe flancul pinionului primei trepte a reductorului din analiza benzilor laterale asociate frecvenţei de angrenare şi valoarea kurtosis şi de asemenea un defect de nealiniere la interfaţa reductor - frână. Sunt extrase forme de undă asociate vibraţiilor generate de defecte. Aceste forme de undă prin forma şi energia lor (raportată la energia GMF) sunt asociate benzilor laterale formate în jurul frecvenţei de angrenare. Se propune într-o lucrare viitoare studiul unor parametri ai ordinelor de vibraţie cu aplicare la detectarea defectelor folosind tehnici de învăţare automată şi inteligenţa artificială.

Iulian LUPEA, Professor Ph.D., Technical University of Cluj-Napoca, Department of Mechanical Systems Engineering, 103-105 Muncii Blvd., 400641 Cluj-Napoca, ☎+40-264-401691, e-mail: Iulian.Lupea@mep.utcluj.ro